Crystallographic phase transition and island height selection in In/Si(111) growth

J. Chen, M. Hupalo, M. Ji, C. Z. Wang, K. M. Ho, and M. C. Tringides*
Department of Physics, Ames Laboratory US, DOE, Iowa Sate University,Iowa 50011, USA

(Received 3 April 2008; published 3 June 2008)

In/Si(111) has been studied with spot profile analysis low-energy electron diffraction, scanning tunneling microscope, and first-principles total energy calculations to identify its growth morphology at low temperatures. Of the different substrate interfaces used, only In growth on Si(111)-Pb-α-$\sqrt{3}\times\sqrt{3}$ has resulted in uniform height fcc (111) four-layer islands. A transition to the bulk bct (101) oriented islands is favored at higher temperatures $T>250$ K and/or larger coverages $\theta>5$ ML. These results suggest two stabilizing effects for the preferred morphologies, i.e., quantum size effects and orientation dependent surface and interface energies. These stabilizing effects are suppported from first-principles calculations.

DOI: 10.1103/PhysRevB.77.233302 PACS number(s): 68.35.Rh, 61.05.jh, 68.37.Ef, 68.60.Dv

As nanostructures become smaller in size, deviations from macroscopic bulk behavior should be expected. The discreteness in their structure and the increasing importance of low symmetry atoms (i.e., the surface atoms in 3D structures, perimeter atoms in 2D structures, etc.) can result in dramatic differences from the structure of macroscopic crystals. A rich and still unexplored realm of potentially technologically relevant metastable phases can be observed as the dimensions of the structures are reduced.[1–5]

Different physical phenomena in reduced dimensions have been realized under a range of conditions for nanostructures smaller than some minimum size. For example, kinetic barriers that control sintering[1] (and therefore catalytic activity) in Pb nanoparticles adsorbed on MgO and 2D Xe adatom or vacancy cluster diffusion[2] on Pt(111) were found to decrease with size, because they are determined by the atoms of the lowest coordination and not by the average curvature of the structure. For metallic islands with heights comparable to the wavelength of the confined electrons λ_F, the island electronic structure is controlled by quantum size effects (QSE).[6–12] More importantly, the confined electron energy can vary as a function of height so preferred island heights were observed. In other systems, different crystallographic phases[13] have been observed in nanostructures, which are different from the bulk phases such as the fcc Fe grown on Cu substrate.[13] During the room temperature growth of Bi on Si(111)-7×7, first islands of a pseudocubic (012) phase grow at low coverage, which convert to the hexagonal bulk structure (001) phase.[14]

In these systems,[1–14] the deviation from bulk behavior on the nanoscale was of only one physical parameter (i.e., lower kinetic barriers so the processes are faster,[1–5] preferred island heights,[6–12] or novel crystallographic phases[13,14]). It would be interesting to find a single nanoscale system where more than one bulk deviation is seen and is controllable with easy experimental "knobs." In this Brief Report, we report that the In growth on the Pb-α-$\sqrt{3}\times\sqrt{3}$ is such a system: four-layer uniform height fcc (111) islands due to the QSE for coverages of less than some critical coverage; the fcc (111) crystallographic phase, which transforms into bulk bct (101) with increasing temperature or coverage; and the enhanced diffusion on this particular Pb-α-$\sqrt{3}\times\sqrt{3}$ interface so mass transport is unusually fast that large islands form at temperatures as low as 150 K. The bct islands prefer to grow in height and can reach multiple heights (i.e., they can easily become many times higher than the deposited amount). Initially, since fcc (111) islands are present and they should convert to bct (101) islands, mixed metastable islands are also observed. It is remarkable that both the uniform height uniformity, the transition from fcc (111) to bct (101), and the fast kinetics well below room temperature are only observed when the growth is on the Si(111)-Pb-$\alpha\sqrt{3}\times\sqrt{3}$ phase (and not on other Si(111) interfaces: clean Si(7×7), In-$\beta\sqrt{3}\times\sqrt{3}$, In-$\sqrt{31}\times\sqrt{31}$, and In-$4\times1$).

These results have been examined in parallel with first-principles total energy calculations to identify the relative contribution of the surface energy, interface energy, and the QSE energy in island stability.

The experiments were performed in two separate UHV chambers. The Si(111) Pb-$\alpha\sqrt{3}\times\sqrt{3}$ phase is prepared by depositing in excess of 1.3 ML of Pb on Si-(7×7) followed by annealing to 500 K. Figure 1(a) shows an area of 500×418 nm^2 at $T=204$ K with $\theta=2.7$ ML of indium grown on Si(111)-Pb $\alpha\sqrt{3}\times\sqrt{3}$ showing uniform height four-layer islands. The islands have a fcc (111) structure as seen directly from their almost hexagonal shape, their height, and as confirmed with diffraction shown below. The corresponding histogram is shown in Fig. 1(b) with an extraordinary sharp height distribution similar to the one observed in the intriguing Pb/Si(111) system. These results are confirmed with the spot profile analysis low-energy electron diffraction,(SPA-LEED), a diffraction measurement that records the variation of the diffracted intensity vs the electron energy as the scattering condition normal to the surface changes from in phase to out of phase. This sharp height distribution of the fcc islands is observed only on Pb-$\alpha\sqrt{3}\times\sqrt{3}$ and the growth on other interfaces leads to a broader distribution of irregularly shaped still fcc In islands.

However, the uniform height selection competes with a different nanoscale effect as the coverage or temperature increases. Figure 2(a) shows a 200×200 nm^2 scanning tunneling microscope (STM) image of the In islands grown on Pb-$\alpha\sqrt{3}\times\sqrt{3}$ at $T=200$ K with $\theta=2.5$ ML. Within this area, a taller island is seen on the top left with a mixed shape, i.e., its left part has a tetragonal (bct phase) and its right part has a trigonal shape (fcc shape). This mixed island does not have a flat top because it contains the same number of layers in the bct and fcc parts. This image shows the onset of a

 ©2008 The American Physical Society

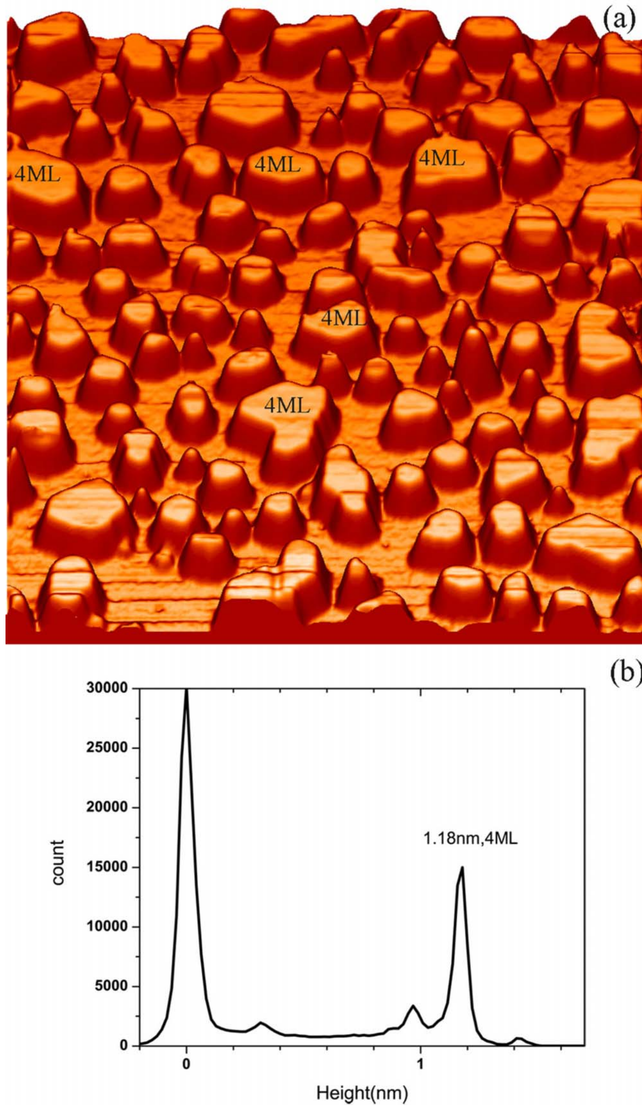

FIG. 1. (Color online) (a) 500×418 nm^2, $T=204$ K, and $\theta=2.7$ ML indium that was grown on Si(111)-Pb-α-$\sqrt{3}\times\sqrt{3}$, showing the uniform height four-layer fcc (111) islands, as seen in the histogram of (b). The absolute measured value of the height is 1.17 nm which corresponds to a nominal 4 layer height as shown on top of a few islands.

crystallographic fcc (111) to bct (101) transition.

Figure 2(b) shows an area of 280×280 nm^2 with the mixed island (located now at the center left of the image) after the stepwise deposition of 2.5 ML. It is remarkable that the mixed island has grown from 10 to 28 ML. This indicates an extraordinary high and selective In mobility, where mass transfer is preferable to the mixed or the bct islands, which quickly grow to larger heights.

These results are fully confirmed by SPA-LEED. The diffraction experiments show that with increasing temperature T or coverage θ. The fcc spots become weaker and eventually disappear while the bct spots grow stronger. Both the 2D and 1D scans are shown in Fig. 3 for the growth at $T=150$ K with an electron energy of 38 eV. Figures 3(a) and 3(c) correspond to $\theta=4$ ML while Fig. 3(b) to $\theta=8$ ML and Fig. 3(d) to $\theta=6$ ML. The red scans are for the clean 7×7 sur-

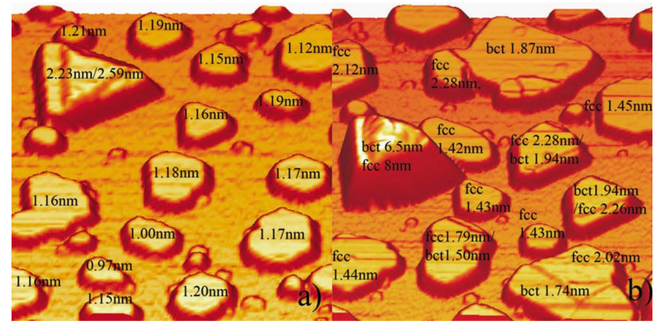

FIG. 2. (Color online) Growth of In on Si(111)-Pb-$\alpha\sqrt{3}\times\sqrt{3}$ at $T=200$ K islands. (a) 200×200 nm^2 and $\theta=2.5$ ML with a fcc (111) island. (b) 280×280 nm^2 and $\theta=5$ ML with fcc (111), bct (101), and mixed islands. The mixed island grew by 18 ML although only 2.5 ML has been deposited.

face and are used for the wave vector calibration. The scanning directions in Fig. 3(c) is $[1\bar{1}0]$, and in Fig. 3(d) the black curve is 4° off the $[11\bar{2}]$ and the red curve is along $[11\bar{2}]$.

These diffraction data directly give the fcc (111) and bct (101) planar unit cells from the spot positions: the fcc (111) spots along $[1\bar{1}0]$ are at 115.2% of the Brillouin zone (BZ) and the bct (110) spots at 4° off the $[11\bar{2}]$ direction are at 98.2% in the BZ. From these planar unit cells, we can deduce the 3D fcc unit cell (the lattice constant is 0.477 nm) and the c axis lattice constant $c=0.495$ nm of the bct 3D unit cell. (From the ratio $c/a=1.52$, we obtain the lattice constant in the other two directions, $a=0.325$ nm). These 3D unit cell sizes indicate that the islands are not strained. From these values, we deduce the interlayer spacing of the fcc (111) planes to be 0.274 nm and the bct (101) planes to be 0.231 nm. The area between the In islands is covered by the α-$\sqrt{3}\times\sqrt{3}$ phase, as seen by the strong (1/3,1/3) and (2/3,2/3) spots, although as concluded from the low coverage experiments, these correspond to the mixed In and Pb "Devil's Staircase" phases. This confirms the tendency of the In-Pb system to form a 2D smooth alloyed phase that has a higher In mobility (than on the 7×7) and can account for the extraordinary speed of building the mixed bct+fcc islands.[15] The characteristic spots at 14% of the Brillouin zone in Fig. 3(a) that are close to the (00) spot originate from the Moire pattern at the interface (8 indium match 7 Si unit cells).

It is well known that the bct crystal structure is the ground state structure of In. Previous first-principles calculations have shown that the energy of bulk fcc In is only slightly higher than the bulk bct by approximately 2 meV/atom.[16] They are sufficiently close for the transition between the two structures to be possible, especially for low dimensional islands at smaller thickness.

In order to verify this competition, first-principles calculations were performed using the plane-wave pseudopotential VASP code.[17] The interactions between the core and valence electrons are described by the projected augmented wave potential.[18] The exchange correlation energy is described by the generalized conjugate gradient approximation using the form proposed by Perdew–Burke–Ernzerhof[19]

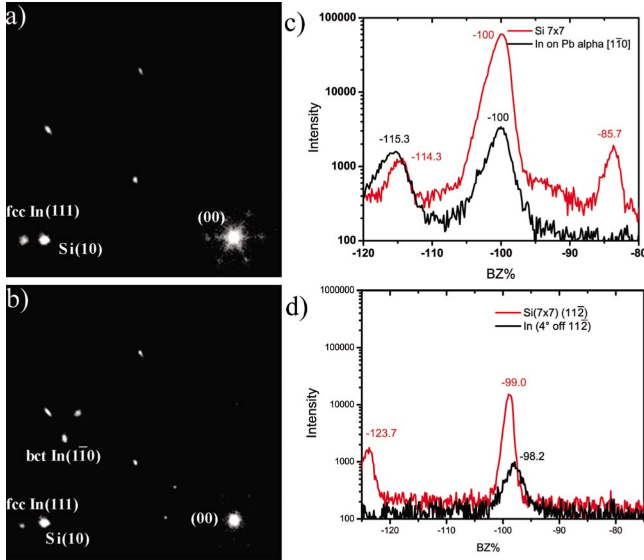

FIG. 3. (Color online) 2D diffraction patterns and 1D scans for the In growth on Si(111)-Pb-$\alpha\sqrt{3}\times\sqrt{3}$ $T=150$ K with an electron energy 38 eV. (a) shows the fcc (111) growth with $\theta=4$ ML, and (b) mixed bct (101) and fcc (111) growth with $\theta=8$ ML. (c) shows 1D scans along $[1\bar{1}0]$ and (d) scans for $\theta=6$ ML 4° off the $[11\bar{2}]$. The red (dark gray) curves are scans of 7×7 spots used for the wave vector calibration.

(PBE). The energy cutoff for the plane-wave basis was 350 eV. The optimized lattice constants from the calculations are 0.331 nm/0.503 nm (i.e., a/c) for the bct bulk structure and 0.48 nm for the fcc structure, which are in good agreement with the experimentally measured ones, i.e., 0.325 nm/0.495 nm and 0.477 nm, respectively. The calculated cohesive energies for the two crystalline structures are −2.7208 and −2.7223 eV per atom, respectively, which is consistent with the previous results.[16] The thin film calculations were performed for the fcc In terminated by the (111) plane and the bct In terminated by the (101) plane, as seen in the experiment. The unit cell used in the calculation is 6.2 nm in the z direction, including the vacuum region normal to the surface and periodic boundary conditions. The thickness of the films varies from 2–19 layers, and a $20\times20\times1$ Monkhorst–Pack k-point mesh was used for Brillouin zone sampling. In all cases, the film was relaxed until the forces were less than 0.1 eV/nm.

The surface energies E_s of the two structures, as a function of thickness, are shown in Fig. 4(a) for the free standing slab calculations. The surface energy of the fcc (111) is lower than the one of the bct (101) but oscillations are seen with film thickness. These oscillations can be attributed to the QSE with the In fcc (111) film being more stable at 4, 7, and 10 ML, and the bct (101) film is more stable at 6 and 15 ML.

In the present calculations, we note that, according to the energy differences between the fcc and bct structures, the fcc to bct transition would be over 100 ML in thickness, which is much larger than the observed one. This difference would be due to the fact that the free standing films are used and not the real Pb-α-$\sqrt{3}\times\sqrt{3}$ substrate. The interface energy is expected to differ for these two interfaces and will affect the

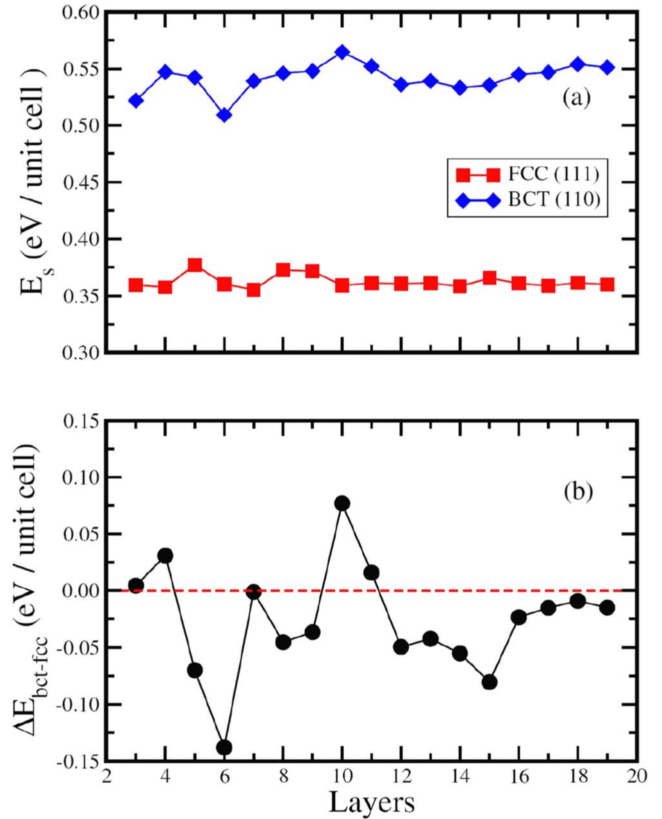

FIG. 4. (Color online) (a) Surface energies $E_s(n)$ of the indium fcc (111) and bct (101) films as a function of thickness n for free standing slab calculations; (b) The difference in energy between the bct (101) and fcc (111) films as a function of n assuming the interface energy difference $\Delta E_i=-0.16$ eV. Within a narrow coverage range at ~8 ML both the bct (101) and fcc (111) films become of preferred energy.

film stability. The total energy of the film can be written as $E(n)=E_s^0+E_i+nE_b+E_{\text{QSE}}(n)$, where n is the number of layers, E_s^0 is the surface energy in the limit of large thickness (so that the QSE is negligible), E_i is the interface energy (between the metal film and the substrate), E_b is the bulk energy (per layer), and the $E_{\text{QSE}}(n)$ is the energy as the function of the film thickness due to the QSE. Then the relative energy between the two film structures is $\Delta E_{\text{bct-fcc}}(n)=\Delta E_s^0+\Delta E_i+n\Delta E_b+\Delta E_{\text{QSE}}(n)$. Using the surface energy of the free standing film from Fig. 4(a) and noting that $E_s=E_s^0+(E_{\text{QSE}})/2$, the ΔE_s^0 and $\Delta E_{\text{QSE}}(n)$ can be estimated. The calculation of the interfacial energy difference between the two film structures is not feasible because the structure of the interface is not known. Since the transition from fcc to bct occurs earlier than the free standing slab prediction, this suggests that the interface energy of the bct film is lower than that of the fcc film on the Pb-α-$\sqrt{3}\times\sqrt{3}$ substrate. If we assume that the interface energy difference between the two structures is $\Delta E_i=-0.16$ eV, then the relative energy of the two structures $\Delta E^{\text{bct-fcc}}(n)$ as a function of the film thickness n can be plotted in Fig. 4(b). The plot shows that there is a strong energetic competition for the growth of fcc and bct thin films below 12 layers, most likely due to the QSE. The bct structure is more favorable above 12 layers.

These calculations are indicative of the ease of transformation of the crystallographic transition with T or θ and the existence of mixed crystals. However, given that in the experiment the fcc islands initially form, any transformation to bct(101) islands should not only be determined by the energy differences but also by the kinetic barriers to be overcome. At low temperatures <200 K, these barriers can account for the extraordinary stability of the four-layer fcc islands below some minimum coverage ~ 4 ML. (The calculation compares two ideal crystal structures and their $T=0$ thermodynamic energy difference).

The earlier results in the literature have indicated partial information on the crystallographic transition. In Ref. 20, indium nanoparticles within Ar gas atmosphere at 300 K were found with x-ray scattering to transform from bct to fcc within the range of 4–6 nm. In Ref. 21, TEM studies under UHV conditions of the indium nanoparticles deposited at room temperature (RT) on carbon films undergo an fcc to bct transition with a crossover size at 6 nm.

The epitaxial growth of indium on Si(111)-7×7 at RT was carried out with a low-energy electron microscopy[22] and STM,[23] showing In(111) islands. At temperatures higher than RT (~ 440 K), large islands with a linear size of more than 1 μm with a rectangular cross section and bct (101) orientation are consistent with the temperature trend of the current experiments.[22] The island density is extremely low, i.e., less than 2 islands/100 μm^2, which indicates the extraordinary mobility of the indium on the wetting layer. The In islands were also studied with scanning tunneling spectroscopy[24] and angle resolved photoelectron spectroscopy[25] to conclude that the electron localization effects originating from the electron correlations are important; and with reflection high-energy electron diffraction[26] to conclude a layer-by-layer growth at 110 K.

In summary, this work on In/Si(111) shows that other metals besides Pb/Si(111) can have similar sharp island height uniformity. The optimal interface is Si(111)-Pb-α-$\sqrt{3}\times\sqrt{3}$ and the preferred height is four layers. In addition, an allotropic fcc to bct transition is observed with a well-defined kinetic pathway how to attain each crystal structure by varying either the temperature and/or the coverage. These results suggest two effects to be responsible, i.e., QSE stabilize height and surface energy stabilize the crystal structure. These conclusions are quantitatively supported with first-principles calculations. This work clearly shows the possibility of manipulating not only the island height but the crystal structure itself and with fast kinetics at such low temperatures.

Work at the Ames Laboratory was supported by the Department of Energy-Basic Sciences under Contract No. DE-AC02-07CH11358. This research used the resources of the National Energy Research Scientific Computing Center, which is supported by the Office of Science of the U.S. Department of Energy under Contract No. DE-AC02-05CH11231.

---

*Corresponding author. FAX: 515 294 0689; tringides@ameslab.gov

[1] C. T. Campbell, S. C. Parker, and D. E. Starr, Science **298**, 811 (2002).
[2] D. S. Sholl and R. T. Skodje, Phys. Rev. Lett. **75**, 3158 (1995).
[3] D. J. Liu and J. W. Evans Phys. Rev. B **66**, 165407 (2002).
[4] F. Nita and A. Pimpinelli, Surf. Sci. **551**, 31 (2004).
[5] Z. Kuntova, Z. Chvoj, and M. C. Tringides, Phys. Rev. B **71**, 125415 (2005).
[6] K. Budde, E. Abram, V. Yeh, and M. C. Tringides, Phys. Rev. B **61**, R10602 (2000).
[7] M. Hupalo, V. Yeh, L. Berbil-Bautista, S. Kremmer, E. Abram, and M. C. Tringides, Phys. Rev. B **64**, 155307 (2001).
[8] W. B. Jian, W. B. Su, C. S. Chang, and T. T. Tsong, Phys. Rev. Lett. **90**, 196603 (2003).
[9] H. Hong, C. M. Wei, M. Y. Chou, Z. Wu, I. Basile, H. Chen, M. Holt, and T. C. Chiang, Phys. Rev. Lett. **90**, 076104 (2003).
[10] A. Mans, J. H. Dil, A. R. H. F. Ettema, and H. H. Weitering, Phys. Rev. B **66**, 195410 (2002).
[11] C. M. Wei and M. Y. Chou, Phys. Rev. B **66**, 233408 (2002).
[12] Z. Y. Zhang, Q. Niu, and C. K. Shih, Phys. Rev. Lett. **80**, 5381 (1998).
[13] A. Kirilyuk, J. Giergiel, J. Shen, M. Straub, and J. Kirschner, Phys. Rev. B **54**, 1050 (1996); A. Biedermann, M. Schmid, and P. Varga, Phys. Rev. Lett. **86**, 464 (2001).
[14] T. Nagao, J. T. Sadowski, M. Saito, S. Yaginuma, Y. Fujikawa, T. Kogure, Y. Hasegawa, S. Hasegawa, and T. Sakurai, Phys. Rev. Lett. **93**, 105501 (2004).
[15] J. Chen, M. Hupalo, and M. C. Tringides (unpublished).
[16] S. I. Simak, U. Haussermann, R. Ahuja, S. Lidin, and B. Johansson, Phys. Rev. Lett. **85**, 142 (2000).
[17] G. Kresse and J. Furthmuller, Phys. Rev. B **54**, 11169 (1996).
[18] G. Kresse and J. Joubert, Phys. Rev. B **59**, 1758 (1999).
[19] J. P. Perdew, K. Burke, and M. Ernzerhof, Phys. Rev. Lett. **77**, 3865 (1996).
[20] A. Yokozeki and G. Stein, J. Appl. Phys. **49**, 2224 (1978).
[21] Y. Oshima, T. Nangou, H. Hirayama, and K. Takayanagi, Surf. Sci. **476**, 107 (2001).
[22] A. Pavloska, E. Bauer, and M. Giessen, J. Vac. Sci. Technol. B **20**, 2478 (2002).
[23] S. L. Surnev, J. Kraft, and F. P. Netzer, J. Vac. Sci. Technol. A **13**, 1389 (1995).
[24] I. B. Altfeder, X. Liang, T. Yamada, D. M. Chen, and V. Narayanamurti, Phys. Rev. Lett. **92**, 226404 (2004).
[25] J. H. Dil, J. W. Kim, T. Kampen, K. Horn, and A. R. H. F. Ettema, Phys. Rev. B **73**, 161308(R) (2006).
[26] M. Strozak, M. Jalochowski, and M. Subotowicz, Acta Phys. Pol. A **81**, 239 (1992).